PAPER

Check for updates

The cation–anion co-exchange in CsPb$_{1-x}$Fe$_x$(Br$_{1-y}$Cl$_y$)$_3$ nanocrystals prepared using a hot injection method

Yue Hu,[a] Yuxin Zhang,[b] Chaoqun Yang,[a] Ji Li[ab] and Li Wang [ID] *[ab]

All inorganic perovskite nanocrystals (NCs) have wide practical applications for their remarkable optoelectronic properties. To obtain blue-emitting perovskites with high photoluminescence quantum yield and room-temperature ferromagnetism, CsPb$_{1-x}$Fe$_x$(Br$_{1-y}$Cl$_y$)$_3$ NCs were synthesized using a hot injection method. The effects of the cation–anion co-exchange on the structural, luminescent and magnetic properties of CsPbBr$_3$ NCs were studied by X-ray diffraction spectroscopy, photoluminescence spectroscopy, transmission electron microscopy, field emission scanning electron microscopy, and vibrating sample magnetometer. The results indicated that there was cation–anion co-exchange in CsPb$_{1-x}$Fe$_x$(Br$_{1-y}$Cl$_y$)$_3$ NCs, while the band-edge energies and PLQY were mainly affected by the anion exchange. The ferromagnetism of CsPb$_{1-x}$Fe$_x$(Br$_{1-y}$Cl$_y$)$_3$ NCs had been observed at room temperature, and there was an increase in saturation magnetization with increasing Fe concentration.

1. Introduction

Since the all-inorganic perovskite (CsPbX$_3$, X = Cl, Br, and I) nanocrystals (NCs) with narrow photoluminescence (PL), high photoluminescence quantum yield (PLQY), and high crystallinity were prepared firstly by Protesescu and co-workers in 2015, more and more attention has been on cesium based perovskite NCs.[1–9] The PLQYs of CsPbBr$_3$ and CsPbI$_3$ NCs are beyond 90% in the green and red spectral ranges, respectively, while that of the blue-emitting NCs is still low.[10–14] Lots of researchers have attempted to solve this question. For example, Ye *et al.* prepared CsPbBr$_3$ quantum dots with a blue PLQY of 68% through controlling the size of NCs. It is unfortunate that the small size (3 nm) caused the agglomeration of the perovskite NCs.[15] At the same time, Zeng *et al.* obtained blue-emitting CsPbBr$_3$ NCs with approximately 100% PLQY, however, it was difficult to cover the whole blue spectrum range.[16] In fact, the optical properties of perovskite NCs can be easily tuned by the individual halide anion exchange to meet the requirements of the new material in optoelectronic applications.[17–22] Thus, the mixed-halide perovskite CsPb(Br$_{1-x}$Cl$_x$)$_3$ NCs can overcome those shortcomings by varying the atomic proportions of Br and Cl, to make their emission wavelength cover the blue spectrum range.

On the other hand, cation doping has been demonstrated as one powerful method for enhancing PLQY. For example, Song *et al.* improved PLQY of the CsPbCl$_3$ quantum dots from 3.2 to 10.3% by doping K$^+$.[23] Zhao *et al.* prepared Mn-doped CsPbCl$_3$ NCs with different Mn concentration prepared in the presence of nickel chloride, which PLQY with orange and red emissions peaked at 600 and 620 nm in hexane were 70% and 39%, respectively.[24] In addition, the doping of some cations can enhance or introduce novel functionalities into quantum dots. Tang and co-workers obtained the triboelectric performance enhancement through doping Ba^{2+} into CsPbBr$_3$ lattice for modulating the microstructures and electrical properties of perovskite films.[25] Li *et al.* observed room-temperature ferromagnetism for Co^{2+} doped CsPbCl$_3$ NCs, and founded the ferromagnetism increased with the increase of Co^{2+} content.[26] Iron ions are not only environment friendly and low cost, but also have good conductivity. Recently, Pradhan *et al.* synthesized Fe^{2+} doped CsPbBr$_3$ perovskite NCs and found that the doped NCs enhanced the catalytic activity compared with undoped CsPbBr$_3$.[27] Singh *et al.*[28] and Wang *et al.*[29] prepared Fe^{3+} and Fe^{2+} doped CsPbCl$_3$ NCs, respectively. It is interesting that they all observed that Fe-doping not only enhanced PLQY, but also improved the homogeneity of size and cubic shape of NCs. In addition, Singh *et al.* prepared Fe:CdSe quantum dots and found the material was superparamagnetic behavior with a weak ferromagnetic exchange interaction, which would open a possibility of understanding the controversial origin of magnetism in diluted magnetic semiconductor quantum dots for future spintronic devices.[30] In this work, to obtain blue-emitting perovskites with high PLQY and room-temperature ferromagnetism, we prepared CsPb$_{1-x}$Fe$_x$(Br$_{1-y}$Cl$_y$)$_3$ NCs using a hot injection method. Interesting variations in luminescent and magnetic properties

[a]Key Laboratory of Functional Materials Physics and Chemistry of the Ministry of Education, Jilin Normal University, Siping 136000, China. E-mail: wangli@jlnu.edu.cn

[b]National Demonstration Center for Experimental Physics Education, Jilin Normal University, Siping 136000, China

Table 1 The actual Fe doping concentration and the values of x for the NCs

PbBr$_2$/FeCl$_2$	1/0	1/0.5	1/1	1/2	1/3
Fe concentration	0%	1.5%	3.6%	8.1%	11.5%
x	0	0.01	0.03	0.07	0.10
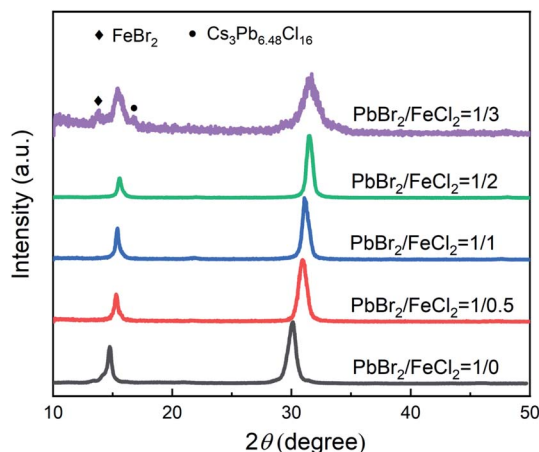
were possible by varying the doping concentration of Fe and Cl. The samples were characterized by various techniques and discussed in detail.

## 2. Experimental

2.1 Materials

Lead bromide (PbBr$_2$, 99.99%), lead chloride (PbCl$_2$, 99.99%), cesium carbonate (Cs$_2$CO$_3$, 99.99%), iron bromide (FeBr$_2$, 99.99%), iron dichloride (FeCl$_2$, 99.99%) and trioctylphosphine (TOP, 90%) were purchased from Aladdin; 1-octadecene (ODE, 90%) was purchased from Alfa Aesar; oleic acid (OA, 90%) and oleylamine (OLA, 70%) were purchased from Aldrich. All chemicals were used without further purification.

2.2 Synthesis of CsPb$_{1-x}$Fe$_x$(Br$_{1-y}$Cl$_y$)$_3$ NCs

The Cs-oleate precursor, CsPbBr$_3$ NCs was synthesized according to the method described by Protesescu et al.[4] For the synthesis of CsPb$_{1-x}$Fe$_x$(Br$_{1-y}$Cl$_y$)$_3$ NCs in a typical procedure, the PbBr$_2$ (0.2 mmol), FeCl$_2$ (α mmol), OLA (1.5 mL), OA (1.5 mL), TOP (1 mL), and ODE (5 mL) were mixed in a 50 mL three-neck round-bottomed flask. After degassed at 110 °C for 20 min, the reaction mixture was heated up to 190 °C under argon flow. 1 mL Cs-oleate precursor was then rapidly injected, and after 15 s, the reaction mixture was cooled by an ice-water bath. The obtained solution was centrifuged at 5000 rpm for 5 min, the

Fig. 1 XRD patterns of CsPb$_{1-x}$Fe$_x$(Br$_{1-y}$Cl$_y$)$_3$ NCs.
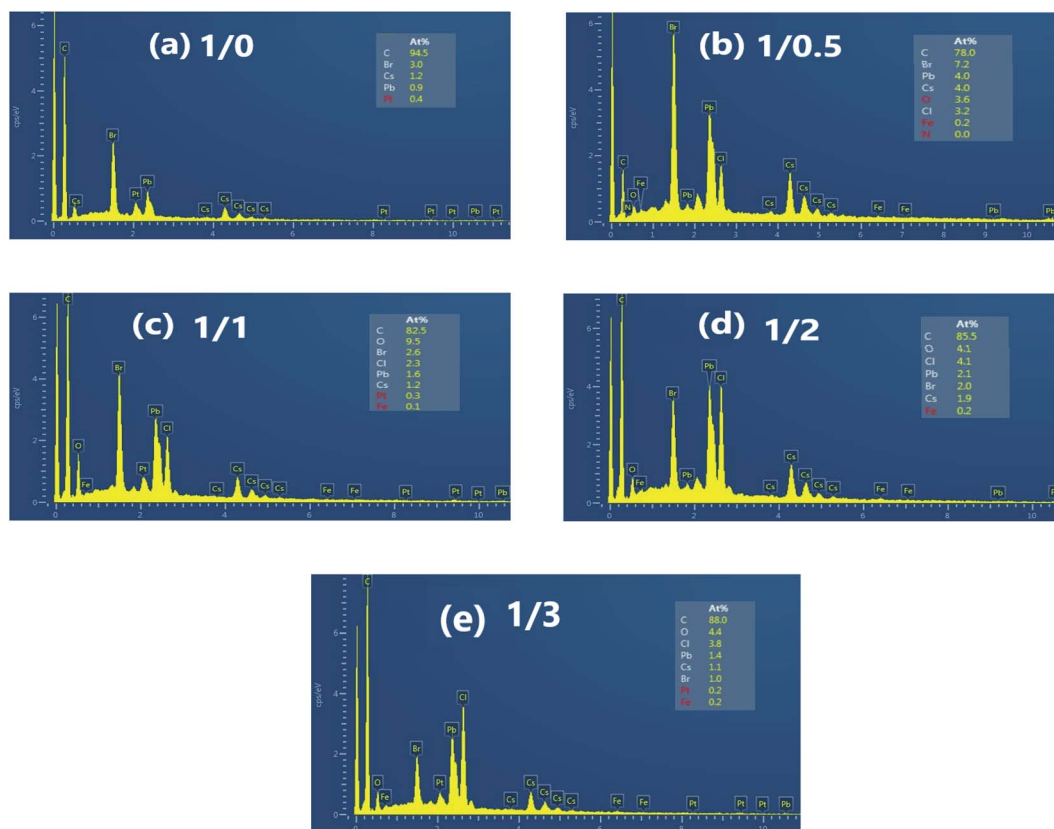
Fig. 2 EDAX spectrum of CsPb$_{1-x}$Fe$_x$(Br$_{1-y}$Cl$_y$)$_3$ NCs with PbBr$_2$/FeCl$_2$ being (a) 1/0, (b) 1/0.5, (c) 1/1, (d) 1/2, and (e) 1/4 (inset: the atomic ratios of the elements).

Table 2 The values of Cl/Br and y from the EDAX spectrum, and the chemical formulas for $CsPb_{1-x}Fe_x(Br_{1-y}Cl_y)_3$ NCs

$PbBr_2/FeCl_2$	Cl/Br	y	$CsPb_{1-x}Fe_x(Br_{1-y}Cl_y)_3$
1/0	0	0	$CsPbBr_3$
1/0.5	0.44	0.31	$CsPb_{0.99}Fe_{0.01}(Br_{0.69}Cl_{0.31})_3$
1/1	0.88	0.47	$CsPb_{0.97}Fe_{0.03}(Br_{0.53}Cl_{0.47})_3$
1/2	2.05	0.67	$CsPb_{0.93}Fe_{0.07}(Br_{0.33}Cl_{0.67})_3$
1/3	3.8	0.79	$CsPb_{0.90}Fe_{0.10}(Br_{0.21}Cl_{0.79})_3$

supernatant was discarded and the particles were dispersed in hexane and centrifuged again to remove the residual reaction mixture. The NCs obtained with the mole ratios of $PbBr_2$ and $FeCl_2$ were 1 : 0, 1 : 0.5.1 : 1, 1 : 2, and 1 : 3, respectively.

2.3 Characterization

The actual doping concentration of Fe, structure and morphology were characterized by an inductively coupled plasma mass spectrometer (ICP-MS, PerkinElmer Nexion 350-X), X-ray diffraction (XRD, Rigaku D/max-2500/PC) with CuKα radiation, transmission electron microscopy (TEM, JEOL-JEM-2100), field emission scanning electron microscopy (FE-SEM,

JEOL JSE-7800F). UV-visible absorption spectra, the steady-state and time-resolved fluorescence spectra an absolute photoluminescence quantum yield were recorded by Shimadzu UV-2700 spectrophotometer, a Horiba Jobin Yvon fluorologo-3 fluorescence spectrometer and Otsuka QE-2000. The magnetic properties were measured by a vibrating sample magnetometer (VSM, Lake Shore 7407).

3. Results and discussion

Table 1 lists the actual doping concentration of Fe relative to Pb for the $CsPb_{1-x}Fe_x(Br_{1-y}Cl_y)_3$ NCs. It reveals a growth in Fe concentration with increasing $FeCl_2$ concentration. In addition, the values of x in the chemical formula $CsPb_{1-x}Fe_x(Br_{1-y}Cl_y)_3$ are listed in Table 1.

Fig. 1 gives the XRD patterns of $CsPb_{1-x}Fe_x(Br_{1-y}Cl_y)_3$ NCs. It is obviously observed there are two strong diffraction peaks at 14.47° and 30.08° for the NCs with $PbBr_2/FeCl_2$ being 1/0, which correspond to (100) an (200) directions of $CsPbBr_3$, respectively. It is the typical cubic structure, being consistent with the standard card (PDF#54-0752). With increasing $FeCl_2$ concentration, the diffraction peaks shift obviously to a larger angle, which is due to the exchange of the large ionic radius of Br^-
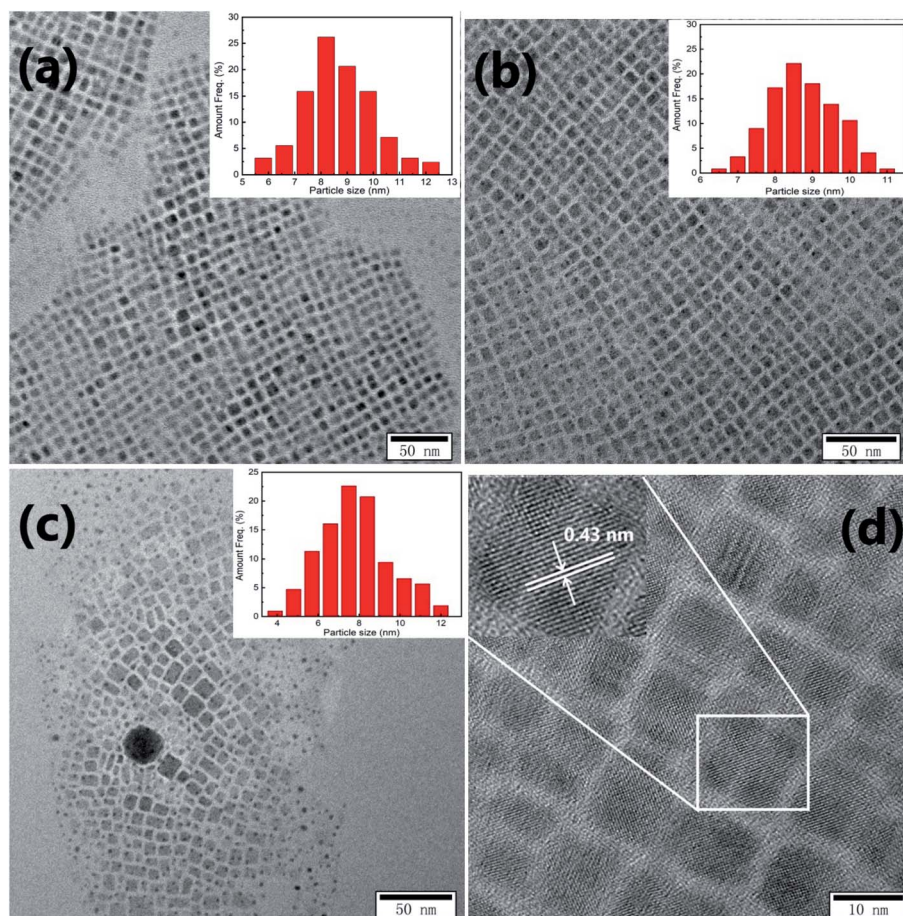
Fig. 3 TEM images of $CsPb_{1-x}Fe_x(Br_{1-y}Cl_y)_3$ NCs with $PbBr_2/FeCl_2$ being (a) 1/0, (b)1/1, and (c) 1/3 (inset: size distribution), and HRTEM image (d) of NCs with $PbBr_2/FeCl_2$ being 1/1 (inset: the high magnification image).

(1.820 nm) to the smaller Cl^- (1.670 nm) and Pb^{2+} (0.119 nm) to Fe^{2+} (0.078 nm). For the NCs with $PbBr_2/FeCl_2$ being 1/3, there are two new peaks at 13.79 °and 16.79° in the XRD pattern. According to the standard card, they are the impurity phases $FeBr_2$ (PDF#15-0829) and $Cs_3Pb_{6.48}Cl_{16}$ (PDF#45-1243). Overall, a certain amount of Cl^- and Fe^{2+} can dope in the $CsPbBr_3$ NCs and the structure is not damaged.

Fig. 2(a–e) is the EDAX spectrum of $CsPb_{1-x}Fe_x(Br_{1-y}Cl_y)_3$ NCs. There are only Cs, Pb and Br elements in the Fig. 2(a), and the atomic ratio of Cs : Pb : Br is 1.2 : 0.9 : 3.0, indicating the $CsPbBr_3$ NCs having been formed. With increasing $FeCl_2$ concentration, Fe and Cl elements appear except for Cs, Pb and Br (seeing Fig. 2(b–e)).

Table 2 shows the values of the atomic ratio Cl/Br and y for $CsPb_{1-x}Fe_x(Br_{1-y}Cl_y)_3$ NCs from the EDAX spectrum. With increasing $FeCl_2$ concentration, Cl/Br and y increase from 0 to 3.8 and 0 to 0.79, respectively. It is worth noting that the value of Cl/Br is larger than that of Fe/Pb obtained from ICP-MS for all NCs, showing there being a relatively large reactivity of the anion exchange compared to the cation exchange. The similar result was reported for Ni doping in $CsPbBr_3$ NCs,[31] which may be due to the halide and counteraction rich surfaces.[32] The chemical formulas for those NCs are shown in Table 2. For example, when the $PbBr_2/FeCl_2$ is 1/0.5, the actual values of Fe/Pb and Cl/Br are 1.5% and 0.44, respectively, and the chemical formula is $CsPb_{0.99}Fe_{0.01}(Br_{0.69}Cl_{0.31})_3$.

Typical TEM images of $CsPb_{1-x}Fe_x(Br_{1-y}Cl_y)_3$ NCs with $PbBr_2/FeCl_2$ being 1/0, 1/1, and 1/3 are shown in Fig. 3(a–c). In Fig. 3(a), the undoped $CsPbBr_3$ NCs have a cubic morphology with an average cube length of 8.3 nm showing homogeneous distribution. When $PbBr_2/FeCl_2$ is 1/1, the size (8.5 nm) and the dispersity these NCs remain identical, as displayed in Fig. 3(b). However, in Fig. 3(c), for the NCs with $PbBr_2/FeCl_2$ being 1/3, the size decreases to 7.4 nm, and the homogeneous distribution is destroyed obviously. Thus, a larger amount of Fe^{2+} doped would damage the dispersity for $CsPb_{1-x}Fe_x(Br_{1-y}Cl_y)_3$ NCs. The similar results have been obtained by Pradhan et al.[27] and Wang et al.[29] Fig. 3(d) is the HRTEM image of $CsPb_{1-x}Fe_x(Br_{1-y}Cl_y)_3$ NCs with $PbBr_2/FeCl_2$ being 1/1. It can be seen that the lattice spacing observed articulately demonstrates the good crystallinity of the synthesized NCs.

Fig. 4(a and b) shows the UV-Visible absorption and steady-state PL spectra of $CsPb_{1-x}Fe_x(Br_{1-y}Cl_y)_3$ NCs. In Fig. 4(a), the exciton absorption band of undoped $CsPbBr_3$ NCs is about 507 nm, and there is a blue shift with increasing $FeCl_2$ concentration. On the other hand, in Fig. 4(b), the exciton PL peak is at 511 with full width at half maximum (FWHM) of 16.7 nm (79.9 meV) for undoped $CsPbBr_3$ NCs. With the cation–anion co-exchange, the peak is located at 477, 454, 431 and 415 nm, with the FWHM of 15.2 nm (82.8 meV), 14.1 nm (85.0 meV), 12.4 nm (82.6 meV) and 11.6 nm (83.6 meV), respectively. The obvious blue shift is caused by the doping of Cl^- ions. For
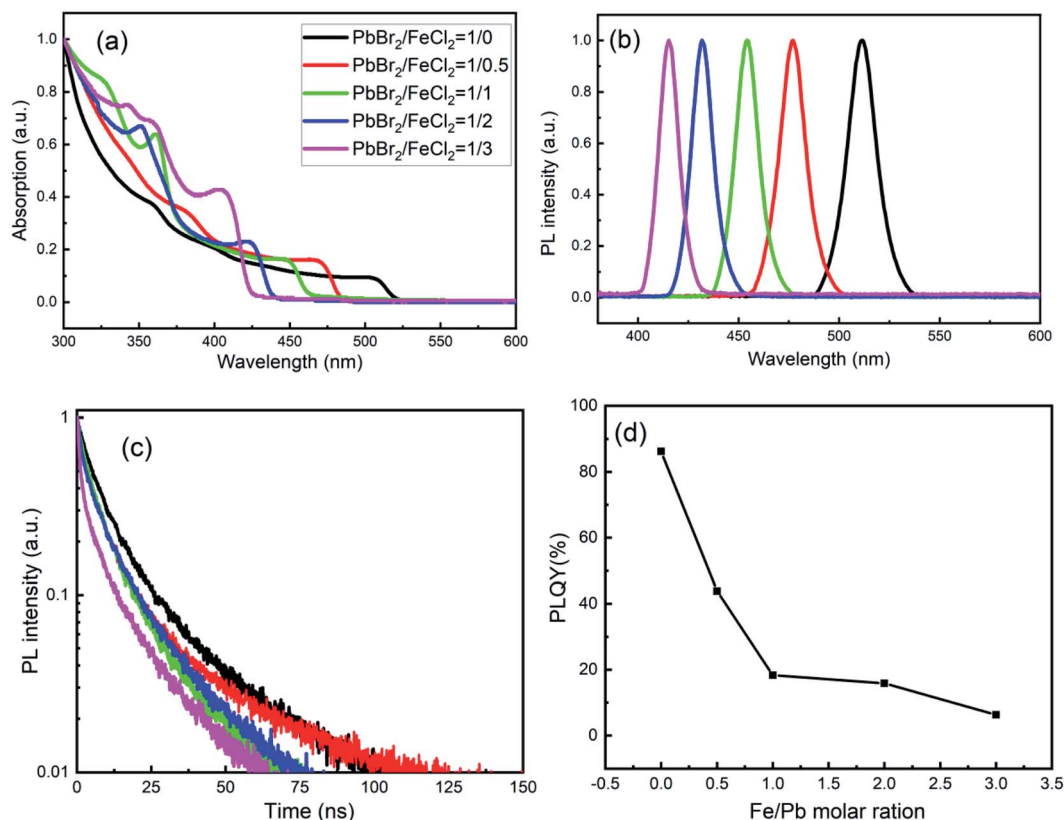

Fig. 4 Absorption (a), PL spectra (b), decay (c) and PLQYs (d) of $CsPb_{1-x}Fe_x(Br_{1-y}Cl_y)_3$ NCs. The solid lines of black, red, green and magenta are corresponding to the NCs with the mole ratios of $PbBr_2/FeCl_2$ being 1/0, 1/0.5, 1/1, 1/2, and 1/3, respectively.

Table 3 PL lifetimes of $CsPb_{1-x}Fe_x(Br_{1-y}Cl_y)_3$ NCs

$PbBr_2/FeCl_2$	A_1	τ_1 (ns)	A_2	τ_2 (ns)	τ_{av} (ns)
1/0	0.652	5.4	0.312	21.7	16.1
1/0.5	0.566	3.4	0.404	13.6	11.0
1/1	0.528	2.1	0.460	13.6	11.8
1/2	0.742	1.1	0.315	12.4	10.4
1/3	0.637	2.5	0.372	9.3	7.2

the NCs with low Fe doping concentration, the decrease in FWHM may be caused by the reduction of defects, while, for the NCs with high Fe doping concentration, it should be caused by the decrease in size of the NCs. Based on the previous reports for mixed chloride-bromide perovskites,[33] those observations in Fig. 4 (a and b) imply there are the cation–anion co-exchange in $CsPb_{1-x}Fe_x(Br_{1-y}Cl_y)_3$ NCs, while the band-edge energies are mainly affected by the anion exchange.

Fig. 4(c) shows the PL decay curves of $CsPb_{1-x}Fe_x(Br_{1-y}Cl_y)_3$ NCs. All decay curves are fitted by a biexponential function: $A(t) = A_1 \exp(-t/\tau_1) + A_2 \exp(-t/\tau_2)$. In the equation, τ_1 and τ_2 are the lifetime constants, while A_1 and A_2 are the PL amplitudes. The average PL lifetime τ_{av} is calculated by formula:[34]

$$\tau_{av} = (A_1 \times \tau_1^2) + (A_2 \times \tau_2^2)/(A_1 \times \tau_1) + (A_2 \times \tau_2) \qquad (1)$$

The values of τ_1, τ_2, A_1, A_2 and τ_{av} are listed in Table 3. The average PL lifetimes of undoped $CsPbBr_3$ NCs was calculated to be about 16.1 ns. The values are lower than that of $CsPbBr_3$ bulk films (about 100 ns), confirming the excitation recombination nature of $CsPbX_3$ NCs. On codoping of Fe^{2+} and Cl^-, τ_{av} decreases compared to the undoped $CsPbBr_3$ NCs, which indicates there are some defects existing in the NCs. And those defects will decrease the PLQY (seeing Fig. 4(d)). In Fig. 4(d), the value of PLQY for the undoped $CsPbBr_3$ NCs is about 86.2%, and then decrease sharply after Fe^{2+} and Cl^- doping. It is known that halide vacancies form shallow trap levels in $CsPbBr_3$ as well as deep trap states in $CsPbCl_3$, which promotes nonradiative

relaxation of the carries and lower the PLQY. Thus the decrease in PLQY is mainly affected by the anion exchange.

Fig. 5 gives the magnetic hysteresis loops measured at room temperature. There is an obvious hysteresis behavior for $CsPb_{1-x}Fe_xCl_3$ NCs. For undoped $CsPbBr_3$ NCs, the saturation magnetization M_s is about 0.14 meum g^{-1}. The small ferromagnetism may be caused by the vacancies and the defects in the NCs.[35] With increasing the concentration of Fe, M_s increases monotonically. The ferromagnetism of $CsPb_{1-x}Fe_x(Br_{1-y}Cl_y)_3$ NCs should be attributed to the doping of Fe^{2+} in the lattice as a substituent for carrier-induced ferromagnetism.[36]

4. Conclusions

In summary, we have studied the luminescent and magnetic properties of $CsPb_{1-x}Fe_x(Br_{1-y}Cl_y)_3$ NCs. The diffraction peak in XRD patterns shift toward a higher 2θ position indicating the successful doping of Fe^{2+} and Cl^- into $CsPbBr_3$ NCs. Although there is cation–anion co-exchange, PL spectra imply the band-edge energies are mainly affected by the anion exchange. The values of τ_{av} and PLQY are smaller than that of undoped $CsPbBr_3$ NCs. In addition, with increasing the concentration of $FeCl_2$, M_s increases monotonically, which should be attributed to the doping of Fe^{2+} in the lattice as a substituent for carrier-induced ferromagnetism. It is fortunate that the $CsPb_{0.99}Fe_{0.01}(Br_{0.69}Cl_{0.31})_3$ NCs obtained have a PLQY of 43.9% at 477 nm and show an obvious room-temperature ferromagnetism, which is of great significance to accelerate the practical application of perovskites in the magneto-optical field.

Conflicts of interest

There are no conflicts to declare.

Acknowledgements

References

1 J. Hieulle, S. Luo, D. Y. Son, A. Jamshaid, C. Stecker, Z. Liu, G. Na, D. Yang, R. Ohmann, L. K. One, L. Zhang and Y. Qi, *J. Phys. Chem. Lett.*, 2020, **11**, 818–823.

2 T. Q. Ma, S. W. Wang, Y. W. Zhang, K. X. Zhang and L. X. Yi, *J. Mater. Sci.*, 2020, **55**, 464–479.

3 Q. S. Chen, J. Wu, X. Y. Ou, B. L. Huang, J. Almutlaq, A. A. Zhumekenov, X. W. Guan, S. Y. Han, L. L. Liang, Z. G. Yi, J. Li, X. J. Xie, Y. Wang, Y. Li, D. Y. Fan, D. B. L. Teh, A. H. All, O. F. Mohammed, O. M. Bakr, T. Wu, M. Bettinelli, H. H. Yang, W. Huang and X. G. Liu, *Nature*, 2018, **561**, 88–93.

4 L. Protesescu, S. Yakunin, M. I. Bodnarchuk, F. Krieg, R. Caputo, C. H. Hendon, R. X. Yang, A. Walsh and M. V. Kovalenko, *Nano Lett.*, 2015, **15**, 3692–3696.
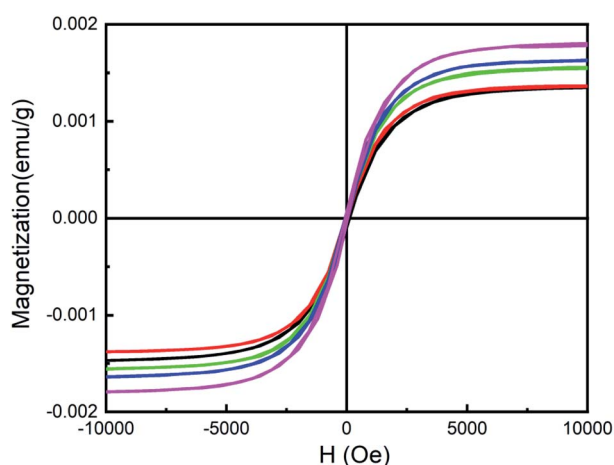
Fig. 5 Hysteresis loops of $CsPb_{1-x}Fe_xCl_3$ NCs at room temperature.

5 A. Pramanik, K. Gates, Y. Gao, S. Begum and R. P. Chandra, *J. Phys. Chem. C*, 2019, **123**, 5150–5156.

6 X. Yuan, X. M. Hou, J. Li, C. Q. Qu, W. J. Zhang, J. L. Zhao and H. B. Li, *Phys Chem Phys*, 2017, **19**, 8934–8940.

7 J. Li, Y. Hu, X. M. Hou, X. Yuan and L. Wang, *Nanotechnology*, 2020, **31**, 085701.

8 X. Li, S. Q. Chen, P. F. Liu, Y. L. Zhang, Y. Chen, H. L. Wang, H. M. Yuan and S. H. Feng, *J. Am. Chem. Soc.*, 2020, **143**, 3316–3320.

9 J. Szeremeta, M. A. Antoniak, D. Wawrzynczyk, M. Nyk and M. Samoc, *Nanomaterials*, 2020, **10**, 1054.

10 F. Liu, Y. H. Zhang, C. Ding, S. Kobayashi, T. Izuishi, N. Nakazawa, T. Toyoda, T. Ohta, S. Hayase, T. Minemoto, K. Yoshino, S. Y. Dai and Q. Shen, *ACS Nano*, 2017, **11**, 10373–10383.

11 J. Pan, Y. Q. Shang, J. Yin, M. D. Bastiani, W. Peng, I. Dursun, L. Sinatra, A. M. El-Zohry, M. N. Hedhili, A. H. Emwas, O. F. Mohammed, Z. J. Ning and O. M. Bakr, *J. Am. Chem. Soc.*, 2018, **140**, 562–565.

12 C. Lou, W. Li, D. Xiong, J. Fu and W. Q. Yang, *Nanoscale*, 2019, **11**, 15206–15215.

13 Y. Zhang, H. O. Zhu, T. W. Huang, Z. P. Song and S. C. Ruan, *Photonics Res*, 2019, **7**, 837–846.

14 C. Chen, Y. J. Wu, L. Liu, Y. B. Gao, X. F. Chen, W. B. Bi, X. Chen, D. L. Liu, Q. L. Dai and H. W. Song, *Adv. Sci.*, 2019, **6**, 1802046.

15 J. Li, L. Gan, Z. S. Fang, H. P. He and Z. Z. Ye, *J. Phys. Chem. Lett.*, 2017, **8**, 6002–6008.

16 Y. Wu, C. Wei, X. Li, Y. Li, S. Qiu, W. Shen, B. Cai, Z. Sun, D. Yang, Z. Deng and H. Zeng, *ACS. Energy. Lett.*, 2018, **3**, 2030–2037.

17 W. Z. Lv, X. X. Tang, L. Li, L. G. Xu, M. G. Li, R. F. Chen and W. Huang, *Phys. Chem. C.*, 2019, **123**, 24313–24320.

18 H. W. Liu, Z. N. Wu, H. Gao, J. R. Shao, H. Y. Zou, D. Yao, Y. Liu, H. Zhang and B. Yang, *ACS. Appl. Mater. Inter.*, 2017, **9**, 42919–42927.

19 J. Li, Y. Hu, J. L. Zhao, X. Gao and L. Wang, *J. Phys. D: Appl. Phys.*, 2019, **52**, 505113.

20 C. Luo, W. Li, D. Xiong, J. Fu and W. Q. Yang, *Nanoscale*, 2019, **11**, 15206–15215.

21 M. A. Uddin, J. D. Glover, S. M. Park, J. T. Pham and K. R. Graham, *Chem. Mater.*, 2020, **32**, 5217–5225.

22 Z. T. Li, C. J. Song, L. S. Rao, H. G. Lu, C. M. Yan, K. Cao, X. R. Ding, B. H. Yu and Y. Tang, *Nanomaterials*, 2019, **9**, 1296.

23 Y. A. Liu, G. C. Pan, R. Wang, H. Shao, H. Wang, W. Xu, H. N. Cui and H. W. Song, *Nanoscale*, 2018, **10**, 14067–14072.

24 K. Xing, X. Yuan, Y. Wang, J. Li, Y. J. Wang, Y. Fan, L. Yuan, K. Li, Z. J. Wu, H. B. Li and J. L. Zhao, *J. Phys. Chem. Lett.*, 2019, **10**, 4177–4184.

25 Y. D. Wang, J. L. Duan, X. Y. Yang, L. Q. Liu, L. L. Zhao and Q. W. Tang, *Nano Energy*, 2020, **69**, 104418.

26 Z. Cao, J. Li, L. Wang, K. Xing, X. Yuan, J. L. Zhao, X. Gao and H. B. Li, *Mater. Res. Bull.*, 2020, **121**, 110608.

27 S. Shyamal, S. K. Dutta and N. Pradhan, *Phys. Chem. Lett.*, 2019, **10**, 7965–7969.

28 P. J. S. Rana, T. Swetha, H. Mandal, A. Saeki, P. R. Bangal and S. P. Singh, *J. Phys. Chem. C*, 2019, **123**, 17026–17034.

29 Y. Hu, X. Y. Zhang, C. Q. Yang, J. Li and L. Wang, *RSC Adv.*, 2019, **9**, 33017–33022.

30 A. N. Yadav, J. K. Bindra, N. Jakhar and K. Singh, *CrystEngComm*, 2020, **22**, 1738–1745.

31 A. Shapiro, M. W. Heindl, F. Horani, M. H. Dahan, J. Tang, Y. Amouyal and E. Lifshitz, *J. Phys. Chem. C*, 2019, **123**, 24979–24987.

32 V. K. Ravi, P. K. Santra, N. Joshi, J. Chugh, S. K. Singh, H. Rensmo, P. Ghosh and A. Nag, *J. Phys. Chem. Lett.*, 2017, **8**, 4988–4994.

33 G. Pan, X. Bai, D. W. Yang, X. Chen, P. T. Jing, S. N. Qu, L. J. Zhang, D. L. Zhou, J. Y. Zhu, W. Xu, B. Dong and H. W. Song, *Nano Lett.*, 2017, **17**, 8005–8011.

34 F. Zhang, H. ZHong, C. Chen, X. G. Wu, X. Hu, H. Huang, J. Han, B. Zou and Y. Dong, *ACS Nano*, 2015, **9**, 4533–4542.

35 A. N. Yadav, J. K. Bindra, N. Jakhar and K. Singh, *CrystEngComm*, 2020, **22**, 1738–1745.

36 J. K. Bindra, G. Kurian, J. H. Christian, J. V. Tol, K. Singh, N. S. Dalal, M. D. Mochena, S. A. Stoian and G. F. Strouse, *Chem. Mater.*, 2018, **30**, 8446–8456.